

TIME-RESOLVED MEASUREMENT OF QUADRUPOLE WAKEFIELDS IN CORRUGATED STRUCTURES*

Chao Lu^{†1,2}, Feichao Fu^{1,2}, Shenggunag Liu^{1,2}, Tao Jiang^{1,2}, Libing Shi^{1,2},
Rui Wang^{1,2}, Dao Xiang^{‡1,2}, Lingrong Zhao^{1,2}, Pengfei Zhu^{1,2},

¹Key Laboratory for Laser Plasmas (Ministry of Education), Shanghai Jiao Tong University, Shanghai, China

² also at Collaborative Innovation Center of IFSA (CICIFSA), Shanghai Jiao Tong University, Shanghai, China

Zhen Zhang, Department of Engineering Physics, Tsinghua University, Beijing, China

Abstract

Corrugated structures have recently been widely used for manipulating electron beam longitudinal phase space and for producing THz radiation. Here we report on time-resolved measurements of the quadrupole wakefields in planar corrugated structures. It is shown that while the time-dependent quadrupole wakefield produced by a planar corrugated structure causes significant growth in beam transverse emittance, it can be effectively canceled with a second corrugated structure with orthogonal orientation. The strengths of the time-dependent quadrupole wakefields for various corrugated structure gaps are also measured and found to be in good agreement with theories. Our work should forward the applications of corrugated structures in many accelerator based scientific facilities.

INTRODUCTION

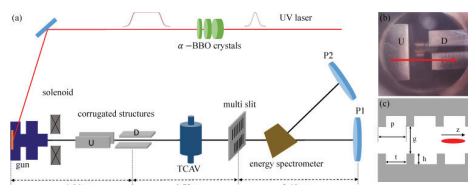


Figure 1: (color online). (a) Schematic layout of the time-resolved measurement of quadrupole wakefields experiment (distances not shown in scale); (b) side view of the CS: upstream CS has a horizontal gap and downstream CS has a vertical gap (the red arrow indicates the beam direction); (c) geometry of the planar CS parameters (the red ellipse represents a beam propagating along the z axis).

When relativistic electron beams pass through metallic pipes or plates with corrugations, electromagnetic waves (wakefields) that propagate with the beams are excited. Such quasi-single frequency radiation on the one hand is a promising candidate for intense THz source (see, for example [1–3]); on the other hand it may be used to manipulate electron beam longitudinal phase space through the interaction between the electron beam and the electromagnetic waves inside the structure (see, for example [4–6]).

* Work supported by the National Natural Science Foundation of China (Grants No. 11327902)

[†] j.j.lucertainfeel@gmail.com

[‡] dxiang@sytu.edu.cn

EXPERIMENT METHODS TO QUANTIFY QUADRUPOLE WAKEFIELDS

Recently the corrugated structures (CS) have been used to tailor beam longitudinal phase space in three different ways, namely removing linear chirp (correlation between beam's longitudinal position and beam energy), removing quadratic chirp and imprinting energy modulation. For instance, when the electron bunch length is much shorter than the wavelength of the wakefield, the beam sees a deceleration field that increases approximately linearly in longitudinal direction when it passes through a CS. This longitudinal wakefield can be used to “dechirp” the beam after bunch compression to reduce beam global energy spread [4–11]. Alternatively, when the electron bunch length is comparable to the wavelength of the wakefield, the beam sees a longitudinal wake that approximates a sinusoid. This wakefield can be used to compensate for the beam quadratic chirp [12–14] that otherwise increases free-electron laser (FEL) bandwidth in seeded FELs (see, e.g. [15]) and degrades the MeV ultrafast electron microscope (UEM) performance [16, 17]. Yet another scenario is when electron bunch length is much longer than the wavelength of the wakefield. In this regime the longitudinal wakefield can be used to produce energy modulation in beam longitudinal phase space that may be further converted into density modulation for producing THz radiation [18–20].

In this paper the beam emittance and transverse phase space in presence of CS are measured with multi-slit method. We show that the time-dependent focusing or defocusing introduced by quadrupole wakefields mainly results in mis-

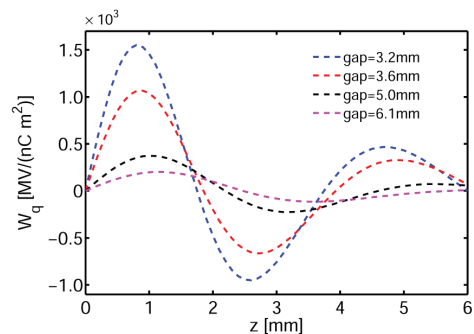


Figure 2: (color online). The point charge quadrupole wake fields at various CS gaps respectively $g = 3.2, 3.6, 5.0, 6.1$ mm.

match in beam slice phase space, leading to considerable growth in beam projected emittance. We also provide definitive evidence through measurement of the beam transverse phase space that indeed if the CS is composed of two identical parts with the second half rotated by 90 degrees with respect to the first half, the quadrupole wakes can be canceled. Furthermore, the strengths of the time-dependent quadrupole wakefields for various CS gaps are also measured and found to be in good agreement with theories. We anticipate that our study should forward the applications of CS in many accelerator facilities.

The experiment is conducted at the Center for Ultrafast Diffraction and Microscopy at Shanghai Jiao Tong University [21]. The schematic layout of the experiment is shown in Fig. 1(a). The bunch quadrupole wakefield (shown in Fig. 2) $w_\lambda(z)$ is given by the convolution between the point charge quadrupole wake field and the beam longitudinal distribution,

$$w_\lambda(z) = \int_0^\infty W_q(s)\lambda(z-s)ds \quad (1)$$

The quadrupole wakefield manifests itself as a time-dependent focusing (defocusing) effect and is related to the focal length f as,

$$1/f(z) = w_\lambda(z)L_c/E \quad (2)$$

where L_c is the length of the CS and E is electron beam energy.

In our experiment the quadrupole wakefields are quantified through measurement of the beam phase space in presence of the CS. When a beam passes through a linear Hamiltonian system, its final beam matrix σ_f is connected with its initial beam matrix σ_i as $\sigma_f = R\sigma_i R^T$, where R is the

symplectic transfer matrix of the system and R^T is transpose of R . Under the thin-lens approximation, the Twiss parameters of the beam before (α_i, β_i and γ_i) and after (α_f, β_f and γ_f) the CS is connected with the CS focusing effect as (see e.g. [22])

$$\begin{bmatrix} \beta_f \\ \alpha_f \\ \gamma_f \end{bmatrix} = \begin{bmatrix} 1 & 0 & 0 \\ 1/f & 1 & 0 \\ 1/f^2 & 2/f & 1 \end{bmatrix} \begin{bmatrix} \beta_i \\ \alpha_i \\ \gamma_i \end{bmatrix} \quad (3)$$

With the beam Twiss parameters measured with the multi-slit method, one obtains the focal length f with Eq. (3). Inserting f into Eq. (2) yields the quadrupole wakefield as

$$w_\lambda(z) = \frac{E}{L_c} \frac{\alpha_f - \alpha_i}{\beta_i} \quad (4)$$

EXPERIMENTAL RESULTS

Cancellation of Time-dependent Quadrupole Wake Fields

With the TCAV on, the streaked beam distributions for various settings of the CS are shown in the top row of Fig. 3, and the corresponding beamlets distributions with the mask inserted are shown in the bottom row of Fig. 3.

Here we give the results for three representative slices (bunch head, bunch center and bunch tail) as indicated by the dashed squares in Fig. 3(a). The phase spaces for the representative slices under various conditions (Fig. 3) are shown in Fig. 4. The slice emittance is about $0.55 \mu\text{m}$ and the projected emittance is about $0.6 \mu\text{m}$ when the two CS are widely open (Fig. 4(a)). Because the phase space ellipse for each slice has approximately the same slope, the projected beam emittance is close to the slice emittance. With the gap of the downstream CS reduced to 3.2 mm, it can be clearly seen that slice phase space rotates clockwise from

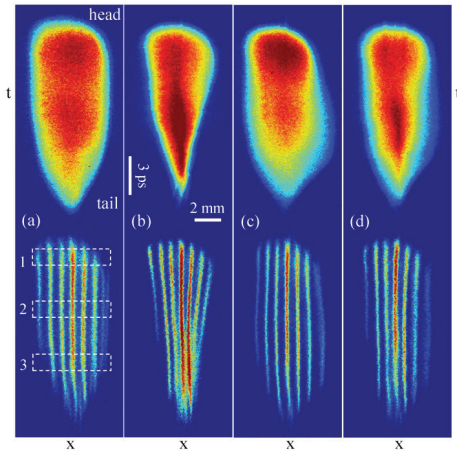


Figure 3: (color online) Time-resolved measurements of beam (top) and beamlets (bottom) distribution on screen P1. Four situations are shown: (a) with two CS widely open; (b) with downstream CS gap set at 3.2 mm; (c) with upstream CS gap set at 3.2 mm; (d) with both CS both gaps set at 3.2 mm. The dashed squares in (a) indicates the three representative slices used for analysis of emittance in Fig. 4.

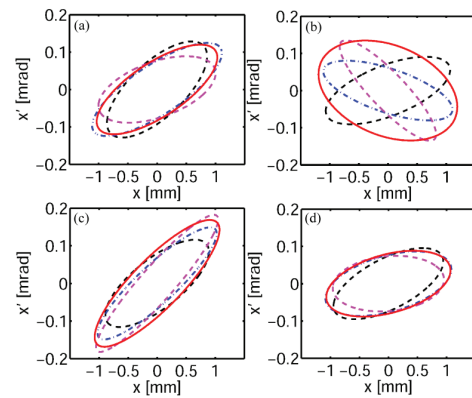


Figure 4: Slice and projected phase space ellipses in four situations respectively: (a) with two CS widely open; (b) with downstream CS gap set at 3.2 mm; (c) with upstream CS gap set at 3.2 mm; (d) with both CS both gaps set at 3.2 mm. The phase spaces for the head slice, central slice and tail slice are shown with dashed black line, dotted dashed blue line and dashed magenta line, respectively. The projected phase space is shown with solid red line.

head to tail (Fig. 4(b)). As a result of this mismatch, the projected beam emittance increases to about $1.0 \mu\text{m}$ (note, the slice emittance is reduced to about $0.50 \mu\text{m}$ because a small fraction of the particles (about 15%) with large offset are collimated by the CS).

Similarly, when the gap of the upstream CS is reduced to 3.2 mm, the time-dependent defocusing wake rotates the slice phase space counter clockwise (Fig. 4(c)). It is worth mentioning that in Fig. 4(c) the projected emittance is measured to be about $0.70 \mu\text{m}$, smaller than that in Fig. 4(b). This is likely due to the fact that the horizontal beta function is smaller in the upstream CS (beam is diverging) such that the emittance growth is less sensitive to the quadrupole wake [23]. Finally, with the gaps of the two CS both set at 3.2 mm, the slice phase ellipses becomes approximately aligned again as shown in Fig. 4(d). Because of the effective cancellation of quadrupole wakefields, the projected beam emittance is reduced to about $0.60 \mu\text{m}$. Note, because of the different beta functions in the upstream and downstream CS, there is still a slight increase of the beam emittance even though the quadrupole wake has essentially the same strength and opposite sign.

In a separate experiment, the gap of the downstream CS was further reduced to about 1.4 mm. In this case a large fraction of the electrons are collimated by the structure and only about 2 pC charge went through. The charge is inferred from the intensity of the beam image at screen P1 where the intensity is calibrated with the Faraday cup without the CS. The streaked beamlets are shown in Fig. 5(a). In this case we used the second mask of which the separation of the slit is $350 \mu\text{m}$. At first glance one might think the quadrupole wake focuses the beam at the head and defocuses it at the tail. However, after second thought one realizes that actually the beam is focused by the wake all the way from head to tail because the horizontal beam size is always smaller than

that at the bunch head. Because the focusing is strongest in the beam center (the beamlets almost overlap in the beam center), the beamlets finally developed to a curved shape.

To clearly show the relative orientation of the slice phase space ellipses, the beam is divided into 9 slices as indicated in Fig. 5(a). As shown in Fig. 5(b) the front five slice phase ellipses rotate clockwise because the focusing strength increases from the bunch head to the bunch center. After reaching the peak value at the bunch center, the focusing strength of the wakefield decreases from bunch center to bunch tail, and as a result the last five slice phase ellipses rotate counterclockwise as shown in Fig. 5(c). The slice emittance is measured to be about $0.20 \mu\text{m}$ (primarily due to the reduced charge) and the projected emittance is about $0.40 \mu\text{m}$.

It is worth mentioning that the emittance grows here by only a factor of 2 even though the gap is reduced to 1.4 mm. This is because the beam charge is also low in this case (wakefield strength is proportional to beam charge). Furthermore, a mirror symmetry (i.e. the bunch tail is similar to the mirror image of the bunch head with respect to the bunch center) is developed in the final beam distribution because the time-dependent quadrupole wake peaks at the bunch center. This reduces the mismatch of the slice phase space and thus leads to reduced emittance growth (e.g. the phase space ellipses for slice 1 and slice 9 have roughly the same slope; similarly slice 2 and slice 8 are also aligned, etc.).

Quadrupole Wake Fields at Various Longitudinal Positions

In addition to studying the effect of quadrupole wakefields on beam emittance growth, here we also present the measurement of the quadrupole wakefield strength. By measuring the phase space for various slices one obtains the Twiss parameters of each slice and the quadrupole wakefield strengths at various longitudinal positions can be quantified with Eq. (4). It should be pointed out that with the multi-slit method it is the beam phase space at the mask that is measured. In our analysis the beam phase space is back propagated to

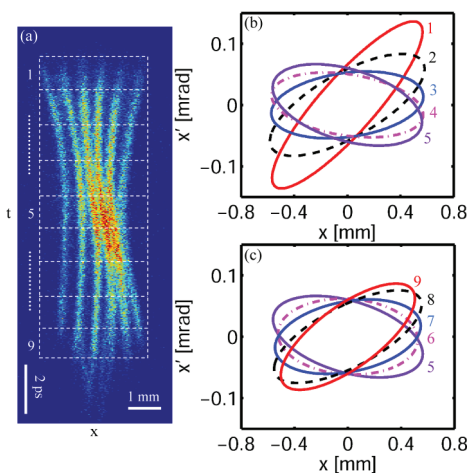


Figure 5: (a) Streaked beam distribution with the gap of the downstream CS reduced to 1.4 mm; (b) Phase space ellipses for the front five slices (from bunch head to bunch center); (c) Phase space ellipses for the latter five slices (from bunch center to bunch tail).

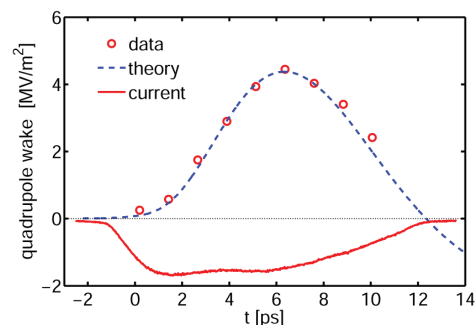


Figure 6: Measured (red circles) and simulated (blue dashed line) time-dependent quadrupole wakefields with the gap of downstream CS set at 3.2 mm. The beam longitudinal distribution is also shown in red solid line.

the center of the CS to obtain the Twiss parameters at the CS. Specifically, the Twiss parameters at the CS obtained without the CS is taken as those “before” the CS (α_i , β_i and γ_i in Eq. (3)), and the Twiss parameters obtained with the CS is taken as those “after” the CS (α_f , β_f and γ_f in Eq. (3)).

With this method the time-dependent quadrupole wakefield for the beam in Fig. 3(b) is shown in Fig. 6. The simulated quadrupole wakefield obtained by convolving the beam longitudinal distribution (red line in Fig. 6) with the point charge quadrupole wake field is also shown in Fig. 6 with the blue dashed line. To match the experimental results, in the simulation the bunch charge is assumed to be 8 pC which is slightly higher than the measured beam charge. This may be due to the fact that the point wake used for analysis (Fig. 3) only considers the dominate modes of the wakefield, and there might be contributions from other modes [24]. Also there could be considerable uncertainty in measurement of the beam charge with our home-made Faraday cup where secondary electron emission is not minimized. Nevertheless, the overall shape and strength of the quadrupole wakefield is in good agreement with the experimental results.

Quadrupole Wake Fields at Various CS Gaps

To study how the quadrupole wakefield scales with the CS gap, we increased the CS gap to 3.6, 5.0 and 6.1 mm. The measured beamlets are shown in the inset of Fig. 7. The quadrupole wakefield strength at the central slice for various CS gaps are obtained through measurement of the Twiss parameters of the central slice. The beam loss is about 5% for $g = 3.6$ mm and is negligible for the other two cases, so the beam longitudinal distribution may be assumed identical. The measured quadrupole wake at various CS gap is normalized to the beam charge ($Q = 5$ pC as for the $g = 3.2$ mm case) and shown with red circles in Fig. 7. The theoretical wakefield strength is then similarly obtained by a convolution of the beam distribution (assuming $Q = 8$ pC)

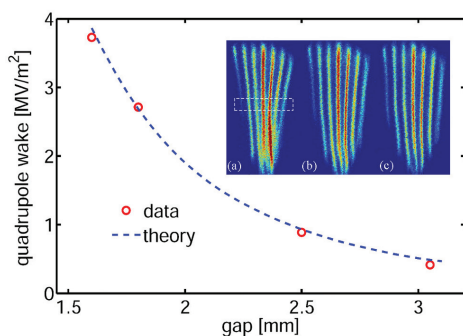


Figure 7: Measured (red circles) and simulated (blue dashed line) quadrupole wakefields of the central slice at various gaps. The streaked beamlets at various CS gaps are shown in the insets [(a) for $g = 3.6$ mm, (b) for $g = 5.0$ mm and (c) for $g = 6.1$ mm]. The dashed square indicates the region of the central slice used for analysis .

with the point wake, and is found to be in good agreement with the experimental results.

CONCLUSIONS

In summary, we provided a complete characterization of the quadrupole wakefield in planar CS. It is demonstrated that while the time-dependent quadrupole wakefield produced by a planar CS causes significant growth in beam transverse emittance, it can be effectively canceled with a second CS with orthogonal orientation. Our work should forward the applications of CS in many accelerator based scientific facilities.

REFERENCES

- [1] K. Bane *et al.*, *Instrum. Methods Phys. Res.*, A 677, 67–73 (2012).
- [2] A.V.Smirnov *et al.*, *Phys. Rev. ST Accel. Beams*, 18, 090703 (2015).
- [3] G. Stupakov, *Phys. Rev. ST Accel. Beams*, 18, 030709, 2015.
- [4] M. Rosing *et al.*, *ANL Report No. WF-144*, 1990.
- [5] P. Craievich, *Phys. Rev. ST Accel. Beams*, 13, 034401 (2010).
- [6] K. L. F. Bane *et al.*, *Nucl. Instrum. Methods Phys. Res.*, Sect. A 690, 106 (2012).
- [7] M. Harrison, G. Andonian *et al.*, *Proc. of PAC2013*, p.291, Pasadena, USA (2013).
- [8] S. Bettoni *et al.*, *Proc. of FEL2013*, p.214, New York, USA (2013).
- [9] S. Antipov *et al.*, *Phys. Rev. Lett.* 112, 034801, 2014.
- [10] P. Emma *et al.*, *Phys. Rev. Lett.* 112, 034801, 2014.
- [11] Z. Zhang, *et al.*, *Proc. of LINAC2012*, p.525, Tel-Aviv, Israel (2012).
- [12] Q. Gu *et al.*, *Proc. of LINAC2012*, p.525, Tel-Aviv, Israel (2012).
- [13] H. Deng *et al.*, *Phys. Rev. Lett.* 113, 254802 (2014).
- [14] F. Fu, *et al.*, *Phys. Rev. Lett.* 114, 114801 (2015).
- [15] E. Hemsing *et al.*, *Phys. Rev. ST Accel. Beams*, 17, 070702 (2014).
- [16] D. Xiang, *et al.*, *Nucl. Instrum. Methods Phys. Res.*, Sect. A 759, 74 (2014).
- [17] R. K. Li *et al.*, *Phys. Rev. Applied*, 2, 024003 (2014).
- [18] S. Antipov *et al.*, *Phys. Rev. Lett.* 108, 144801 (2012).
- [19] S. Antipov *et al.*, *Phys. Rev. Lett.* 111, 134802 (2013).
- [20] F. Lemery and P. Piot, *Phys. Rev. ST Accel. Beams*, 17, 112804 (2014).
- [21] F. Fu *et al.*, *Rev. Sci. Instrum.* 85, 083701 (2014).
- [22] M.G. Minty and F. Zimmermann, *Measurement and control of charged particle beam*, Springer, 2003.
- [23] K. Bane and G. Stupakov, SLAC Report No. SLAC-PUB-15852 (2013).
- [24] A. Novokhatski, *Phys. Rev. ST Accel. Beams* 18, 104402 (2015).